Plasma-enhanced chemical vapor deposition of nanocrystalline diamond

Available online at www.sciencedirect.com
ScienceDirect
Science and Technology of Advanced Materials 8 (2007) 624–634
SCIENCE AND TECHNOLOGY OF ADVANCED MATERIALS
www.elsevier.com/locate/stam

Review

Plasma-enhanced chemical vapor deposition of nanocrystalline diamond

Katsuyuki Okada*

National Institute for Materials Science, 1-1 Namiki, Tsukuba, Ibaraki 305-0044, Japan

Received 12 June 2007; received in revised form 8 August 2007; accepted 27 August 2007
Available online 22 October 2007

Abstract

Nanocrystalline diamond films have attracted considerable attention because they have a low coefficient of friction and a low electron emission threshold voltage. In this paper, the author reviews the plasma-enhanced chemical vapor deposition (PE-CVD) of nanocrystalline diamond and mainly focuses on the growth of nanocrystalline diamond by low-pressure PE-CVD. Nanocrystalline diamond particles of 200–700 nm diameter have been prepared in a 13.56 MHz low-pressure inductively coupled $CH_4/CO/H_2$ plasma. The bonding state of carbon atoms was investigated by ultraviolet-excited Raman spectroscopy. Electron energy loss spectroscopy identified sp^2-bonded carbons around the 20–50 nm subgrains of nanocrystalline diamond particles. Plasma diagnostics using a Langmuir probe and the comparison with plasma simulation are also reviewed. The electron energy distribution functions are discussed by considering different inelastic interaction channels between electrons and heavy particles in a molecular CH_4/H_2 plasma.

Keywords: Low-pressure inductively coupled plasma; Nanocrystalline diamond; UV Raman spectroscopy; Resonance Raman scattering; High-resolution electron energy loss spectroscopy; Electron energy loss spectroscopy; sp^2/sp^3 chemical mapping; Langmuir probe; Direct simulation Monte Carlo; Electron energy distribution function

Contents

1. Introduction

Covalently bonded disordered thin-film materials have been of considerable interest from both fundamental and

*Tel.: +81 29 860 4322; fax: +81 29 852 7449.
E-mail address: okada.katsuyuki@nims.go.jp

1468-6996/$ - see front matter © 2007 NIMS and Elsevier Ltd. All rights reserved.
doi:10.1016/j.stam.2007.08.008

applied perspectives in the last 20 years since the chemical vapor deposition (CVD) of diamond was developed, followed by that of fullerenes and carbon nanotubes [1,2]. Among them, amorphous and nanostructured carbon films are currently being extensively studied for use as electron emitters, cold-cathode sources, and hard low-friction coatings. From the fundamental perspective, on the other hand, the structure of these materials contains both threefold-coordinated (sp^2-bonded) and fourfold-coordinated (sp^3-bonded) carbon atoms. Nanocrystalline diamond films have also attracted attention [3] because they have a low coefficient of friction and a low electron emission threshold voltage. The small grain size (approximately 5–100 nm) gives films valuable tribological and field-emission properties comparable to those of conventional polycrystalline diamond films. Furthermore, applications for micro-electro-mechanical systems (MEMS) devices, metal-semiconductor field effect transistors (MESFETs), electrochemical electrodes, and biochemical devices that take advantage of these excellent properties have been proposed [4–6].

Recent dry plasma processes (e.g., deposition, coating, etching) require a wide area and high-density plasma at low pressures (<1 Torr) [7]. An electron cyclotron resonance (ECR) plasma was first developed to satisfy these conditions. Subsequently, a helicon-wave-excited plasma was employed. It was found [8] that the density of an inductively coupled plasma (ICP) becomes high at low pressures. Amorim et al. [9] reported that the plasma density of ICP after the transition from a low-density E-discharge to a high-density H-discharge reaches $10^{12}\,cm^{-3}$. It is necessary in plasma-enhanced chemical vapor deposition (PE-CVD) to obtain sufficient radical flux for deposition. Thus, ICP is thought to be promising for use in PE-CVD at low pressures.

In this review article, the author's own studies on the synthesis of nanocrystalline diamond by low-pressure ICP-CVD and its spectroscopic characterization are mainly described. Plasma diagnostics using a Langmuir probe and the comparison with plasma simulation are also reviewed.

2. Growth of nanocrystalline diamond

2.1. Conventional microwave PE-CVD

A microwave plasma is most commonly used for the PE-CVD of diamond films [10], in which the conventional pressure of deposition is approximately 20–50 Torr. A CH_4/H_2 mixture, in which the CH_4 content ($[CH_4]$) is usually less than 5%, leads to μm-size polycrystalline diamond films. One method of synthesizing nanocrystalline diamond films is to increase $[CH_4]$ to up to 10% while the substrate temperature is kept constant [11–13]. The resultant morphology changes from faceted microcrystals to spherical nanocrystals.

Another method is to substitute a noble gas for hydrogen while $[CH_4]$ is kept constant. Gruen and co-workers [14,15] demonstrated the synthesis of nanocrystalline diamond films in a CH_4/Ar or C_{60}/Ar microwave discharge, without the addition of hydrogen. Extensive characterization by X-ray diffraction (XRD) analysis, transmission electron microscopy (TEM), and electron energy loss spectroscopy (EELS) showed [16] that the films consisted of a pure crystalline diamond phase with grain size ranging from 3 to 20 nm. They also proposed from plasma diagnostics [17] and theoretical calculations [18] that C_2 dimers may be responsible for the growth of the very fine-grained diamond films, whereas CH_3 radicals are generally believed to be a precursor for the diamond growth.

Recently, Philip et al. [4] reported the deposition of nanocrystalline diamond films under the conventional deposition conditions for μm-size polycrystalline diamond films. The substrate pretreatment by the deposition of a thin H-terminated a-C film followed by the seeding of nanodiamond powder increased the nucleation density on the Si substrate to over $10^{12}/cm^2$. The resultant films were grown to thicknesses ranging from 100 nm to 5 μm, and the thermal conductivity ranged from 2.5 to 12 W/cm K.

In addition to microwave plasma, direct current (dc) [19], hot filament [20], magnetron sputtering [21], and radio frequency (rf) plasmas [22–24] have been utilized for nanocrystalline diamond deposition. Amaratunga et al. [23,24], using CH_4/Ar rf plasma, reported that single-crystal diffraction patterns obtained from nanocrystalline diamond grains all show {1 1 1} twinning.

The stability of nanocrystalline diamond has been discussed from the theoretical point of view by several authors. Badziag et al. [25] pointed out, from the results of semiempirical quantum chemistry calculations, that sufficiently small nanocrystalline diamond (3–5 nm in diameter) may be more stable than graphite due to the formation of C–H bonds at the growing surface. Barnard et al. [26] performed *ab initio* calculations on nanocrystalline diamond of up to approximately 1 nm in diameter. The results revealed that the surfaces of cubic crystals exhibit reconstruction and relaxation comparable to that of bulk diamond, while the surfaces of octahedral and cubo-octahedral crystals show a transition from sp^3 to sp^2 bonding.

2.2. Low-pressure PE-CVD

While a microwave plasma is most commonly used for the PE-CVD of diamond films, ECR plasma is the only plasma used for diamond deposition at pressures below 1 Torr [27–29]. Bozeman et al. [30] reported diamond deposition at 4 Torr using a planar ICP, and there are a few reports that describe the synthesis of diamond by low-pressure ICP. Okada and co-workers [31–33] first reported the synthesis of nanocrystalline diamond particles in a low-pressure $CH_4/CO/H_2$ ICP, followed by Teii and Yoshida [34] using the same gas-phase chemistry.

In the PE-CVD of diamond films, oxygen is added to a CH_4/H_2 system to obtain a high growth rate and/or an improvement of the quality of the resultant films [35–38]. Several authors have discussed the role of oxygen in diamond growth. Mucha et al. [37] pointed out that the addition of oxygen to a CH_4/H_2 system increases the concentration of atomic hydrogen; correspondingly, the formation of amorphous and graphitic carbon, which would otherwise inhibit diamond growth, is suppressed. From a detailed chemical kinetics model that describes both gas phase and surface processes occurring in diamond CVD, Frenklach and Wang [38] postulated that OH radicals and atomic oxygen gasify sp^2 carbon and suppress the formation of aromatic species in the gas phase. Teii and co-workers [39,40] pointed out that the OH radicals resulting predominantly from loss reactions between by-product O atoms and H_2 and CH_4 molecules strongly enhance diamond growth.

A 13.56 MHz low-pressure ICP system [31–33] has been utilized as a source of radicals for PE-CVD and applied to prepare diamond films from a CH_4/H_2 plasma. CO was added to a CH_4/H_2 plasma to clarify the effect of oxygen-containing radicals on diamond growth. A schematic view of the apparatus is shown in Fig. 1. It consists of a water-cooled quartz tube surrounded by a Teflon tube and a stainless-steel growth chamber. An ICP was generated by applying a 13.56 MHz rf power of 1 kW to a three-turn helical coil wound around the Teflon tube. The chamber was pre-evacuated to 5×10^{-5} Torr using a turbomolecular pump (200 l/s). The electrostatic (capacitive) coupling from the rf coil to the plasma in a low-pressure ICP causes contamination due to the etching of the quartz tube. To reduce the electrostatic coupling, a Faraday shield was inserted between the rf coil and the quartz tube. A grounded copper plate with slits at regular intervals along the azimuthal direction was wrapped around the quartz tube. A substrate holder was manipulated from the top of the chamber. Molybdenum plates and silicon (1 0 0) wafers (ϕ 10 mm) were used as the substrate. The substrate was heated using a tungsten filament. The substrate temperature (T_s) was monitored using a sheathed thermocouple and maintained at a prescribed temperature within ± 1 °C using a proportional integral derivative (PID) controller. The deposition conditions were as follows. The flow rates of CH_4 and H_2 were maintained at 4.5 and 75 sccm, respectively, whereas the flow rate of CO ([CO]) was 0, 1.0, or 10 sccm. The total gas pressure (Pr) was varied from 45 to 50 mTorr. T_s was maintained at 900 °C. The deposition duration was 2 h.

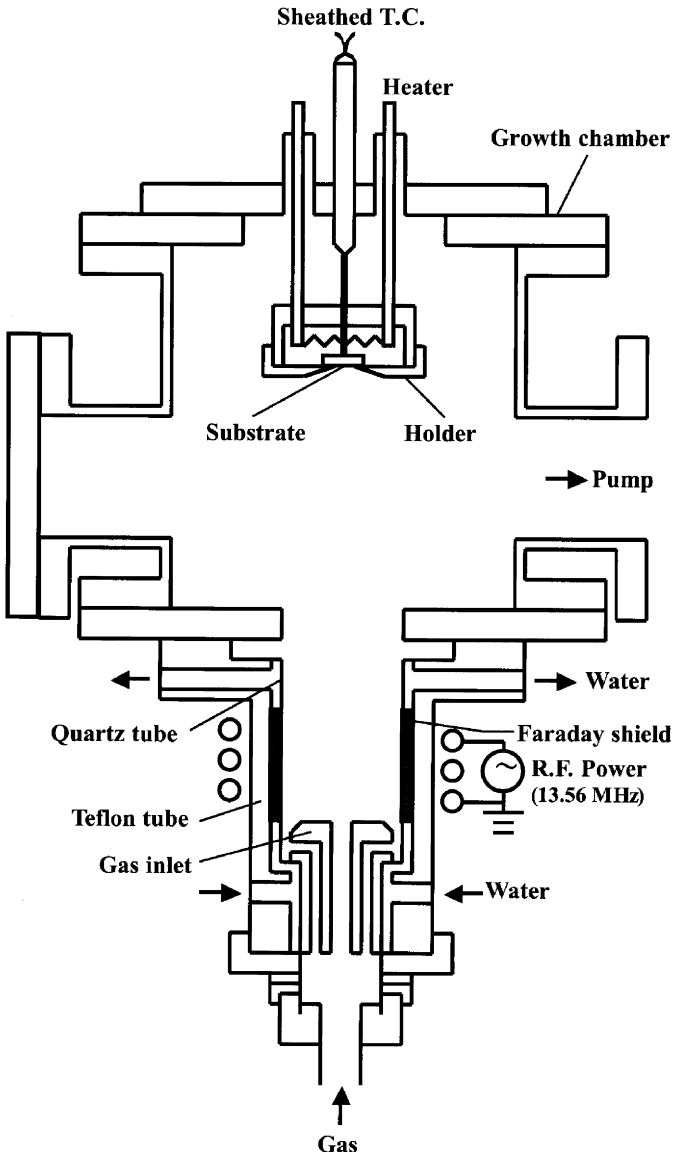

Fig. 1. Schematic description of low-pressure inductively coupled rf plasma CVD system.

3. Spectroscopic characterization

3.1. SEM

Fig. 2 shows SEM photographs of the resultant deposits on a Si(1 0 0) substrate. Figs. 2(a)–(c) correspond to [CO] = 0, 1.0, and 10 sccm, which are referred to as samples A, B, and C, respectively. The morphology of sample A was scale like, as shown in Fig. 2(a), and no crystal facets were clearly seen. When CO was added to the CH_4/H_2 plasma, particles of 200–300 nm diameter, as well as scale-like deposits appeared, as shown in Fig. 2(b). With the increase in [CO], only particles were deposited on the Si substrate, as shown in Fig. 2(c). The diameters of the particles were 200–700 nm. Detailed observation reveals that the particles consist of small particles of about 20–50 nm diameter, and that the particle size remains are almost the same regardless of increasing [CO]. It is therefore speculated that increasing [CO] results in a large supersaturation degree of carbon; thus, the number of encounters between particles is increased.

The addition of CO to CH_4/H_2 plasmas is considered to produce oxygen-containing radicals, e.g., atomic oxygen, OH radicals, and CO radicals themselves in the plasmas.

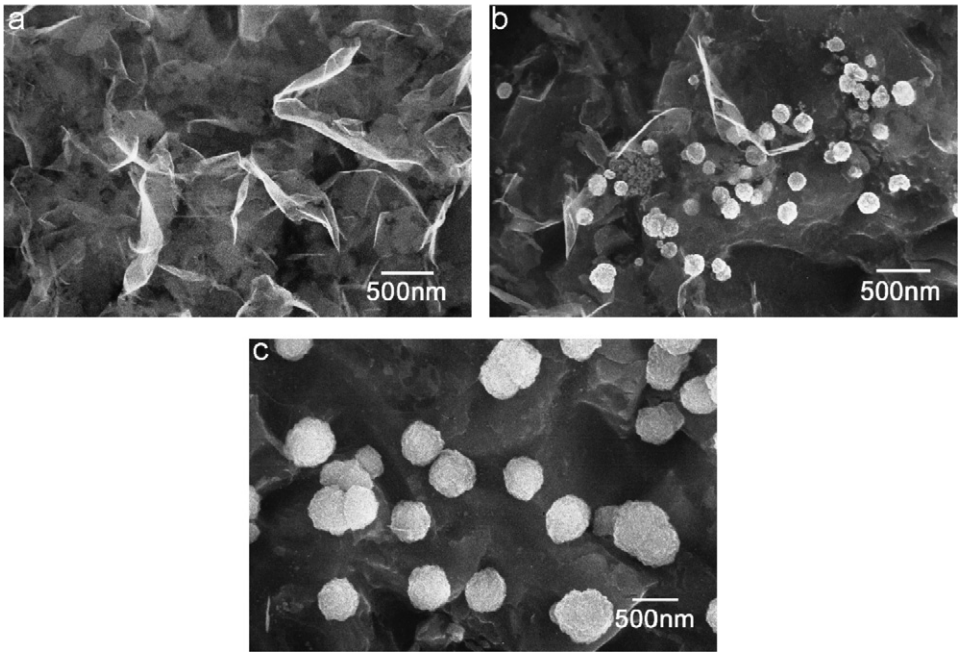

Fig. 2. SEM micrographs of obtained deposits: (a) $[CH_4]/[CO] = 4.5/0$ sccm, (b) $[CH_4]/[CO] = 4.5/1.0$ sccm, and (c) $[CH_4]/[CO] = 4.5/10$ sccm.

As mentioned above, a morphological change from a scale-like deposit to the deposition of particles took place upon adding CO. Also, the number of encounters between particles increased with an increase in [CO]. According to the TEM and XRD patterns [33], nondiamond carbon was effectively removed with an increase in [CO]. We therefore presume that oxygen-containing radicals produced by the addition of CO play an effective role in the removal of nondiamond carbon under diamond growth conditions and that the CO additive results in a large supersaturation degree of carbon. This is consistent with the previously reported hypotheses [37,38] that OH radicals and atomic oxygen gasify sp^2 carbon and that they suppress the formation of amorphous carbon and graphitic carbon.

3.2. Raman spectroscopy

Raman spectroscopy is a nondestructive method of studying the vibrational band structure of materials. It has been extensively used for the characterization of diamond [41–44], graphite [45], and diamond-like carbon (DLC) [42,43,46–49]. Raman scattering is the most popular technique for identifying sp^3 bonding in diamond and sp^2 bonding in graphite and DLC. Although Raman scattering should represent the phonon density of states (PDOS) weighted by a coupling parameter, Raman spectroscopy of sp^2-bonded carbon with an excitation wavelength in the visible range (514, 488 nm, etc.) does not provide a good representation of the PDOS [50]. Since the local sp^2-bonded carbon energy gap of ~2 eV is comparable to the energy of visible Raman excitation, the sp^2-bonded carbon network exhibits electronic π–π^* transition resonance enhancement in the Raman cross-section [43,48–50]. On the other hand, sp^3-bonded carbon does not exhibit such a resonance effect because of the higher local gap of ~5.5 eV. As a result, the Raman spectra obtained using visible excitation are completely dominated by sp^2-bonded carbon. However, Raman spectroscopy with ultraviolet (UV) excitation has recently been used for characterizing DLC [50–53]. The advantage of UV Raman spectroscopy is that it eliminates the resonance effect of sp^2-bonded carbon. Excitation of 244 nm (5.1 eV) is far from the energy of the previously mentioned sp^2-bonded carbon resonance. It is thus expected that the resonance Raman scattering from sp^2-bonded carbon is suppressed and that the signal from sp^3-bonded carbon may be increased. UV Raman spectra of tetrahedral amorphous carbon (t-aC) films containing sp^3 bonding predominantly exhibit a peak at ~1150 cm^{-1} attributed to an sp^3-bonded carbon network [50–52]. Okada et al. [54] first applied UV Raman spectroscopy to the characterization of the bonding structures of nanocrystalline diamond. Sun et al. [55] reported the UV Raman characteristics of nanocrystalline diamond films for grain sizes 120–28 nm. They pointed out that the downshift and broadening of the diamond peak with decreasing grain size are consistent with the phonon confinement model. On the other hand, Prawer et al. [56] reported the visible Raman spectra for nanocrystalline diamond powder with grains of ~5 nm diameter. The peaks at 500, 1140, 1132, and 1630 cm^{-1} are compared with the calculated vibrational density of states (VDOS) of diamond, and the origin of features in the vibrational spectrum obtained from nanocrystalline diamond has been hypothesized.

In Raman measurements [57], the 514 nm line of an Ar^+ laser, the 325 nm line of a He–Cd laser, and the 244 nm line of an intracavity frequency-doubled Ar^+ laser were

employed. The incident laser beam was directed onto the sample surface under a backscattering geometry at room temperature. For the 514 nm excitation, the scattered light was collected and dispersed in a SPEX 1403 double monochromator and detected using a photomultiplier. The laser output power was 300 mW. For the 325 and 244 nm excitation, the scattered light was collected using fused-silica optics and analyzed using a UV-enhanced CCD camera with a Renishaw micro-Raman System 1000 spectrometer modified for use at 325 and 244 nm, respectively. A laser output of 10 mW was used, which resulted in an incident power at the sample of approximately 1.5 mW. The spectral resolution was approximately 2 cm^{-1}. It was verified that no photoalteration of the samples occurred during the UV laser irradiation by confirming that the visible Raman spectra were unaltered after the UV Raman measurements.

Fig. 3 shows the 514-nm-excited Raman spectra. Figs. 3(a)–(c) correspond to samples A, B, and C, respectively. The Raman spectrum of sample A exhibits two peaks at ~1355 cm^{-1} (*D* peak) and ~1580 cm^{-1} (*G* peak) assigned to sp^2 bonding [45]. New peaks appear at ~1150 and ~1480 cm^{-1} in sample B. The former peak is due to sp^3 bonding. Nemanich and co-workers [42,44] assigned the peak at ~1150 cm^{-1} to microcrystalline or amorphous diamond. Prawer and Nugent [58] attributed the peak at 1100–1150 cm^{-1} to the surface phonon mode of diamond from EELS studies of nanophase diamond powder. On the other hand, Ferrari and Robertson [59] have recently proposed another interpretation, that the peak at ~1150 cm^{-1} is not attributed to nanocrystalline diamond but to the sp^2 bonding of a *trans*-polyacetylene oligomer of a given conjugation length. The peak at ~1480 cm^{-1} is probably related to amorphous sp^2 structures [44], although it is downshifted from the *G* peak. Both *D* and *G* peaks become relatively small compared with those of sample A. The peak at ~950 cm^{-1} is derived from scattering by two transverse-optical (TO) phonons of the silicon substrate [43]. The incident laser beam reached the substrate because the substrate was not fully covered by the deposit, as shown in Fig. 2(b). In the Raman spectrum of sample C, the *G* peak becomes a shoulder and the *D* peak becomes faint, while the peak at ~1480 cm^{-1} has the highest intensity and the peak at ~1150 cm^{-1} still remains. However, the three spectra in Fig. 3 do not clearly exhibit the 1332 cm^{-1} diamond peak. These features of the Raman spectra imply that the deposit due to CH_4/H_2 predominantly contains sp^2 bonding; the addition of CO to CH_4/H_2 produces a mixture of sp^2 and sp^3 bonding; an increase in [CO] brings about an increase in sp^3 bonding. These trends are consistent with the TEM and XRD observations, which reveal that the increase in [CO] improves the crystallinity of the deposit.

Fig. 4 shows a sequence of Raman spectra from sample C for different excitation wavelengths. Figs. 4(a)–(c) correspond to 514, 325, and 244 nm, respectively. In contrast with the spectrum obtained from 514 nm excitation, the 325-nm-excited Raman spectrum exhibits a clear peak at 1332 cm^{-1} and a marked enhancement of the peak at ~1580 cm^{-1}, while the peak at ~1150 cm^{-1} becomes a shoulder. In the 244-nm-excited Raman spectrum, only the peak at 1332 cm^{-1} is enhanced, whereas the peak at ~1580 cm^{-1} is weakened. Neither peak nor shoulder can be recognized at ~1150 cm^{-1}. The Raman spectrum in Fig. 4(a) is superimposed on a broad photoluminescence background. This background diminishes with increasing excitation photon energy as shown in Figs. 4(b) and (c).

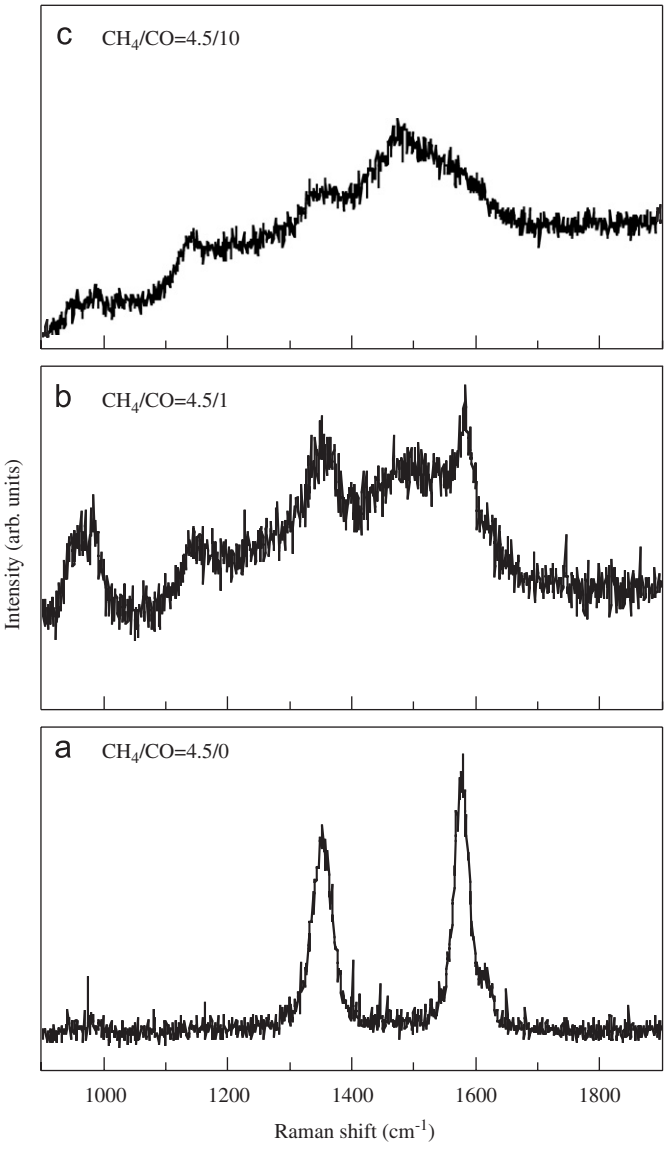

Fig. 3. The 514-nm-excited Raman spectra of obtained deposits for different gas mixtures: (a) $[CH_4]/[CO] = 4.5/0$ sccm, (b) $[CH_4]/[CO] = 4.5/1.0$ sccm, and (c) $[CH_4]/[CO] = 4.5/10$ sccm.

The TEM and XRD patterns revealed [33] that the deposit is not amorphous carbon but nanocrystalline diamond. Nonetheless, the 514-nm-excited Raman spectra do not exhibit a clear diamond peak at 1332 cm^{-1}, although the peak due to the sp^3-bonded carbon network appears at ~1150 cm^{-1}. The Raman cross-section of the

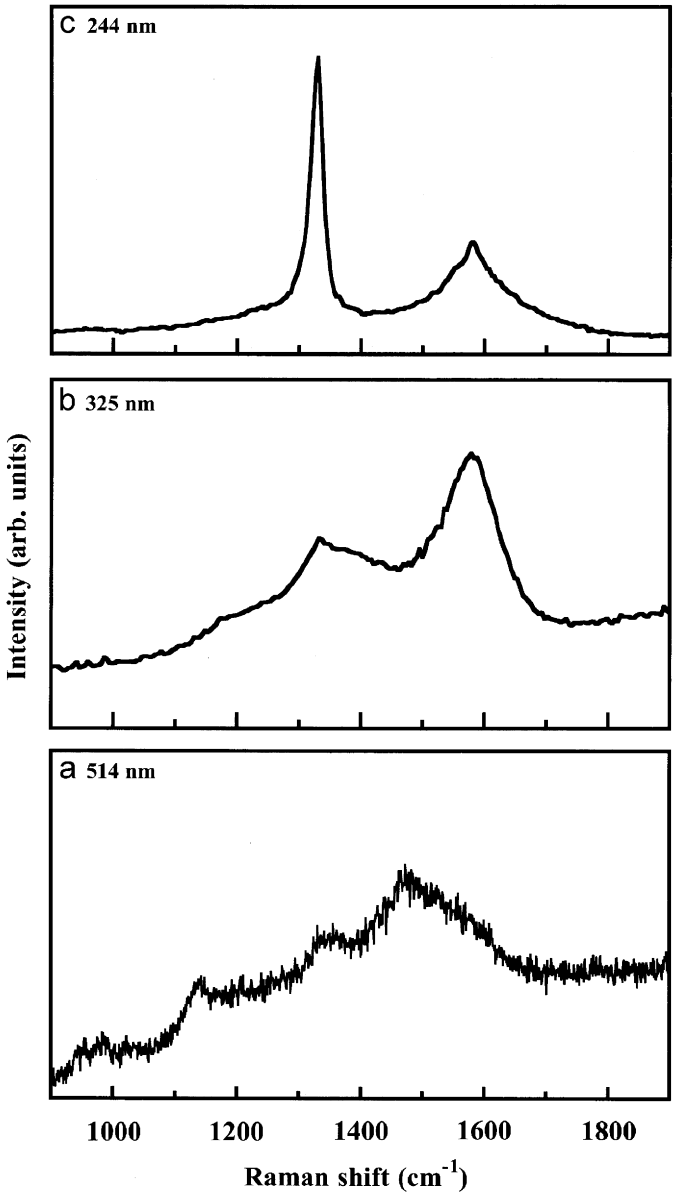

Fig. 4. Raman spectra of sample C ([CH_4]/[CO] = 4.5/10 sccm) for different excitation wavelengths: (a) 514 nm, (b) 325 nm, and (c) 244 nm.

sp^2-bonded carbon network is resonantly enhanced under visible excitation [43,48–50], which consequently causes the 1332 cm^{-1} diamond peak to overlap with the peaks due to sp^2-bonded carbon.

The suppression of the resonance Raman effect, which was dominant in the 514 nm excitation, and the possible increase in the signal from sp^3-bonded carbon are expected to occur at higher photon energies. Wagner et al. [43] reported that the resonance enhancement due to scattering by sp^3-bonded carbon is expected at the incident photon energy of 4.8 eV, which is close to the onset of the σ–σ^* transition in both sp^2- and sp^3-bonded carbon. Gilkes et al. [51] stated that the 244 nm photon energy is sufficient to cause the σ–σ^* transition at both sp^2 and sp^3 sites. The enhancement of the peaks at both 1332 and ~1580 cm^{-1} under the 325 nm excitation suggests that the resonance enhancement of the Raman cross-section due to sp^2-bonded carbon still remains and that the σ–σ^* transition in both sp^2- and sp^3-bonded carbon is possibly induced. The marked enhancement of the peak at 1332 cm^{-1} and the diminution of the peak at ~1580 cm^{-1} under the 244 nm excitation reveals that the resonance Raman effect due to sp^2-bonded carbon is suppressed whereas the resonance enhancement due to the σ–σ^* transition of sp^3-bonded carbon is mainly attained.

The 244-nm-excited Raman spectra of t-aC films exhibit a peak at ~1150 cm with intensity proportional to the amount of sp^3 bonding in the films [50,51]. However, the diamond peak at 1332 cm^{-1} is enhanced in this study because the obtained deposit is not amorphous carbon but nanocrystalline diamond. The peak at ~1150 cm^{-1} probably disappeared because of the marked enhancement of the diamond peak at 1332 cm^{-1}.

3.3. HREELS

High-resolution electron energy loss spectroscopy (HREELS) is a method of studying the vibrational motion of atoms and molecules on and near the surface by the analysis of the energy spectrum of backscattered low-energy electrons [60]. With developments in modern ultrahigh-vacuum (UHV) technology and increasing interest in the physical properties of clean and adsorbate-covered surfaces and of the chemical phenomena occurring on these surfaces, scientific interest in HREELS has increased rapidly and it has been widely used in recent years [60–65].

HREELS experiments [66] were performed in a UHV chamber. The chamber was pre-evacuated using polyphenylether-oil diffusion pump to a base pressure of ~2×10^{-8} Torr. The HREELS spectrometer consisted of a double-pass electrostatic cylindrical-deflector-type monochromator and the same type of analyzer. The energy resolution of the spectrometer was 4–6 meV (32–48 cm^{-1}). A sample was transferred from the ICP growth chamber to the HREELS chamber under atmospheric conditions. It was attached to a small tantalum plate, which was suspended by tantalum wires. The sample was radiatively heated in vacuum by a tungsten filament placed behind the sample. The sample temperature was measured using an infrared ($l = 2.0\,\mu m$) optical pyrometer. All HREELS measurements were taken at room temperature. The electron incident and detection angles were both 72° to the surface normal. The primary electron energy was 15 eV.

Fig. 5 shows the HREELS spectra of the heated films. Figs. 5(a)–(c) correspond to samples A, B, and C, respectively. In Fig. 5(a), without the CO additive, the spectrum has a faint peak at ~1500 cm^{-1} derived from the C=C stretching mode of threefold-coordinated carbon atoms [60]. The spectrum is similar to that of a single-crystal graphite (0 0 0 1) surface [63]. With the CO additive, as shown in Fig. 5(b), one can see a peak at ~1100 cm^{-1}, which is assignable to the C–C stretching

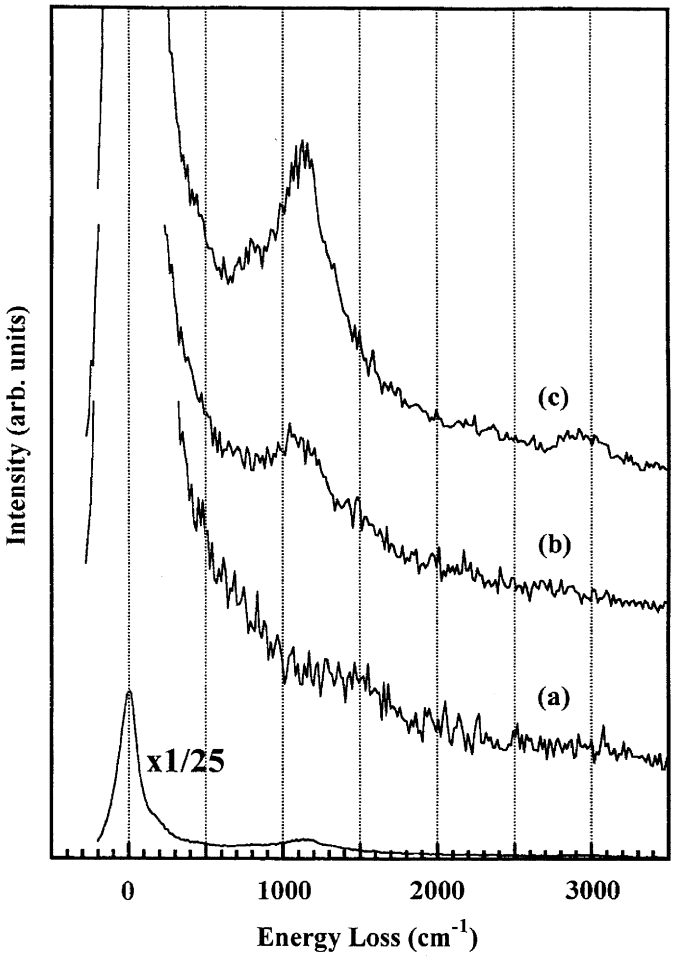

Fig. 5. HREELS spectra of nanocrystalline diamond and diamondlike carbon films with various $[CH_4]/[CO]$. (a) $[CH_4]/[CO] = 4.5.0/0$, (b) $[CH_4]/[CO] = 4.5/1.0$, and (c) $[CH_4]/[CO] = 4.5/10$ sccm. The elastic peak for (c), reduced by a factor of 25, is shown for comparison.

mode of fourfold-coordinated carbon atoms [42,60]. The peak at $\sim$1500 cm^{-1} disappeared. With increasing [CO], as shown in Fig. 5(c), the intensity of the peak at $\sim$1100 cm^{-1} increased. In addition, a shoulder centered at $\sim$700 cm^{-1} appeared. These features of the VDOS are consistent with the theoretical results for random-network models of t-aC. Tight binding molecular dynamics (TBMD) simulations for a sample with 75% fourfold-coordinated atoms predict two major broad peaks at $\sim$700 and $\sim$1100 cm^{-1}, respectively, corresponding to the bending and stretching vibrations in the network [67]. A similar form of the PDOS is obtained from *ab initio* calculations with 90% sp^3 bonding [68].

According to the characterizations by TEM and XRD [33], the sample prepared from a CH_4/H_2 plasma was composed of nanocrystalline diamond and disordered microcrystalline graphite. Then, nondiamond carbon was effectively removed with an increase in [CO]. It is therefore concluded that the VDOS of the nanocrystalline diamond and DLC films extracted from the HREELS data is qualitatively in agreement with the characterizations by TEM and XRD. Although HREELS probes only the near-surface region, this agreement suggests that the surface dynamics do not differ significantly from those of the bulk.

3.4. EELS mapping

The use of EELS in TEM has been demonstrated to be a powerful technique for performing microanalysis and studying the electronic structure of materials [69]. The energy loss near-edge structure (ELNES) is sensitive to the crystal structure. The C-K edges of diamond and graphite are typical examples for ELNES. For trigonal sp^2-bonded carbon, the spectrum within the first 30 eV of the edge can be separated into two broad features, corresponding to the π^* states between 282 and 288 eV and the σ^* states between 290 and 320 eV, whereas for tetrahedral sp^3-bonded carbon only the σ^* peak is observed between 289 and 320 eV [70]. Therefore, one can easily distinguish between diamond and diamond-like carbon by analyzing the ELNES. Muller et al. [71] acquired a mapping of sp^2 and sp^3 states across the silicon–diamond interface by scanning transmission electron microscopy (STEM) and parallel-acquisition electron energy loss spectroscopy (PEELS). Bruley's two-window technique [72] of integrating the intensities of the π^* and σ^* peaks has been used to quantitatively analyze the sp^2 content in the samples. Bursill and co-workers [73–75] carefully performed structural analysis on nanocrystalline diamond powder and studied the surface and bulk plasmon response derived from the low-loss spectra using high-resolution TEM (HR-TEM)/PEELS and STEM/PEELS. Prawer and co-workers [56,76] also reported the EEL spectra of nanocrystalline diamond synthesized by detonation and ion implantation.

HR-TEM observations [77] were performed using a Hitachi HF-3000 at 297 keV, and EELS measurements [77] were carried out using a postcolumn energy filter (GATAN, GIF2002). The vacuum in the microscope had a pressure of less than 1.2×10^{-6} Pa, to ensure that the samples were not contaminated with carbon during TEM observations. Two-dimensional arrays of a charge-coupled device (CCD) were used for digitally recording the TEM images, EEL spectra, and chemical maps. The typical CCD readout times were 5 s for acquiring EEL spectra and 50 s for chemical mappings. The energy resolution of the instrument was approximately 0.5 eV, which was defined as the zero-loss full-width at half-maximum (FWHM).

Fig. 6(a) shows an HR-TEM image of the outer part of a nanocrystalline diamond particle. Lattice fringes clearly appeared in the enlargement of the left-hand side of the sample, as shown in Fig. 6(b). The d value was 0.206 nm, corresponding to the (1 1 1) spacing of diamond. The diffractogram derived from the Fourier transformation of the HR-TEM image exhibited a ring pattern, which means that the observed sample is polycrystalline. Furthermore, careful observation revealed that the particle consisted of smaller subgrains of approximately 20–50 nm diameter. Thus, the boundaries are not surface steps of a single crystal. The size of subgrains is comparable to the grain

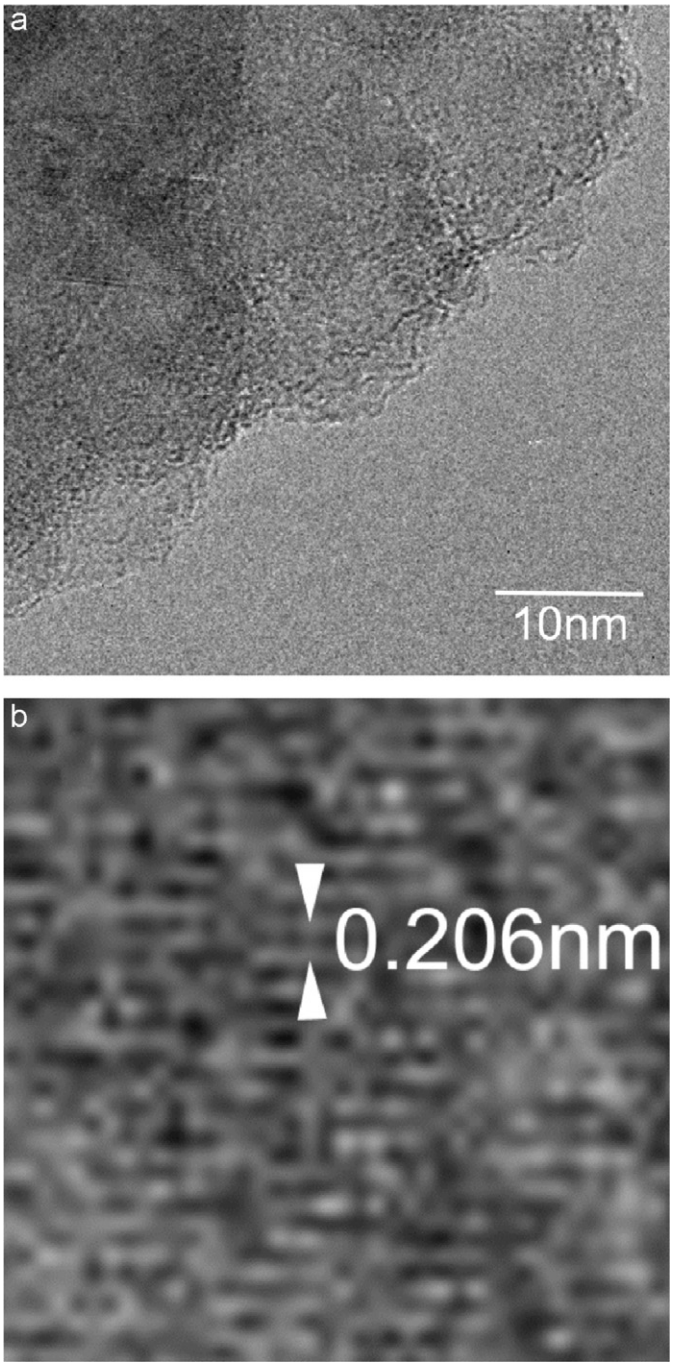

Fig. 6. (a) HR-TEM image of outer part of nanocrystalline diamond particle and (b) enlargement of the left-hand side of (a).

sizes of nanocrystalline diamond films previously reported by several authors [15,23,29,78], in which the grain sizes were found to be in the range 3–50 nm.

The EEL spectrum corresponding to Fig. 6(a) is shown in Fig. 7. It exhibits a peak at 290 eV corresponding to σ^* states and a small peak appears at ~285 eV corresponding to π^* states. The ELNES above 290 eV is similar to that of diamond [70] and is clearly different from that of graphite or sp^3-rich tetrahedral amorphous carbon [72]. The intensity of the π^* peak is much lower than that of the

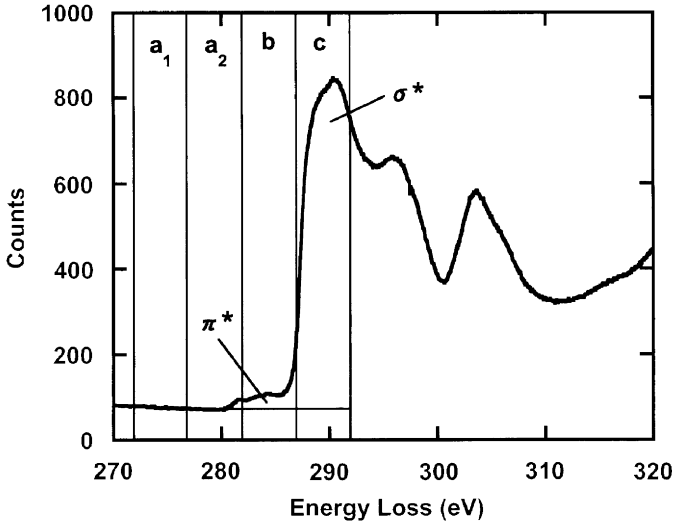

Fig. 7. EEL spectrum corresponding to Fig. 6(a). $\mathbf{a_1}$, $\mathbf{a_2}$, **b**, and **c** indicate the four energy windows 272–277, 277–282, 282–287, and 287–292 eV, respectively.

σ^* peak. Although the σ^* peak in general includes contributions from both sp^2 and sp^3 bonding, the σ^* peak of the EEL spectrum in Fig. 7 is considered to be mainly due to sp^3 bonding. The use of a narrow energy window positioned on the ELNES signal allows the mapping of the variation in intensity as a function of position within the microstructure. The conventional so-called three-window method [69] was employed to remove the background contribution. Two pre-edge images (272–277 and 277–282 eV), indicated by $\mathbf{a_1}$ and $\mathbf{a_2}$ in Fig. 7, were used to obtain an extrapolated background image. The subtraction of the extrapolated background image from the postedge images (282–287 and 287–292 eV) indicated by **b** and **c** produces the π^* and σ^* images, respectively, with the background contribution removed.

The π^* and σ^* images corresponding to the TEM image of Fig. 6(a) are shown in Figs. 8(a) and (b), respectively. Since the intensity of the π^* image was weak compared with that of the σ^* image, the former was increased by a factor of 5. The π^* image reveals that the intensity is strong around the subgrains, whereas the σ^* image shows that the intensity is strong within the subgrains. Although sp^2-bonded graphitic layers do not clearly appear because of the limitation at the resolution of the HR-TEM image, these energy-filtered π^* and σ^* images imply that sp^2 bonding is localized around 20–50 nm subgrains. The sp^2 bonding around the subgrains is considered to contribute to the small peak at ~285 eV in the ELNES. The width of the sp^2 bonding is estimated to be approximately 1 nm from the π^* image in Fig. 8(a). Fallon and Brown [79] reported the presence of amorphous carbon at the grain boundaries of CVD diamond films by TEM observation and EELS analysis. The amorphous carbon is shown to contain almost exclusively sp^2 bonding and to be non-hydrogenated. It was also demonstrated from the theoretical point of view [80] that sp^2 bonding is energetically

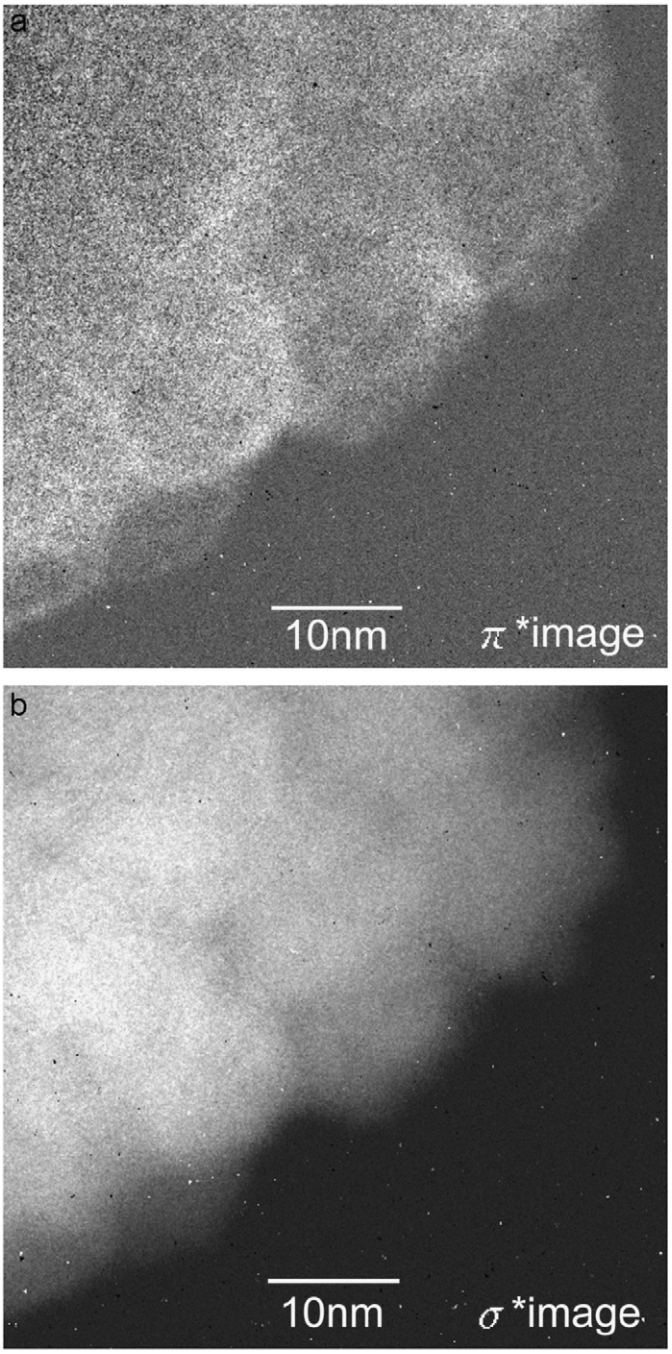

Fig. 8. (a) π^* image corresponding to Fig. 6(a), and (b) σ^* image corresponding to Fig. 6(a).

stable in the grain boundaries of nanocrystalline diamond. It is consequently considered that the sp^2 bonding is localized in the grain boundaries of 20–50 nm subgrains.

4. Plasma diagnostics and simulation

Electron energy distribution functions (EEDFs) are the most informative characteristics of gas discharge plasmas. They define not only plasma macro-parameters such as plasma density and effective electron temperature, but also the rates of plasma chemical microprocesses such as dissociation, attachment, excitation, and ionization, and the fluxes of ions and electrons to the plasma boundary surface [81]. EEDFs are connected directly with the chemistry of the electronic kinetic processes within bulk plasma, and implicitly with the internal parameters. In the absence of more reliable data for inelastic cross-sections corresponding to different reaction channels, the use of EEDFs is the only method of obtaining a better insight into the kinetic processes within the bulk plasma. In low-pressure rf discharges, electrons are not in equilibrium with molecules and ions, which results in a significant deviation of EEDFs from the equilibrium Maxwellian distribution.

Langmuir probe and quadrupole mass spectrometry have been applied to measure plasma parameters, EEDFs, and ion energy distributions (IEDs) of ICP [82,83]. Numerical simulations of the ICP using the direct simulation Monte Carlo (DSMC) method and electron Monte Carlo simulation have also been performed to compare the EEDFs obtained by simulation with measured ones. The EEDFs are discussed by considering the different inelastic interaction channels between electrons and heavy particles in the molecular CH_4/H_2 plasma.

A Langmuir probe (Smart Probe; *Scientific Systems, Inc.*) was utilized to measure plasma parameters and EEDFs in the low-pressure ICP-CVD system. The height of the reactor was 110 mm. A three-turn helical coil was

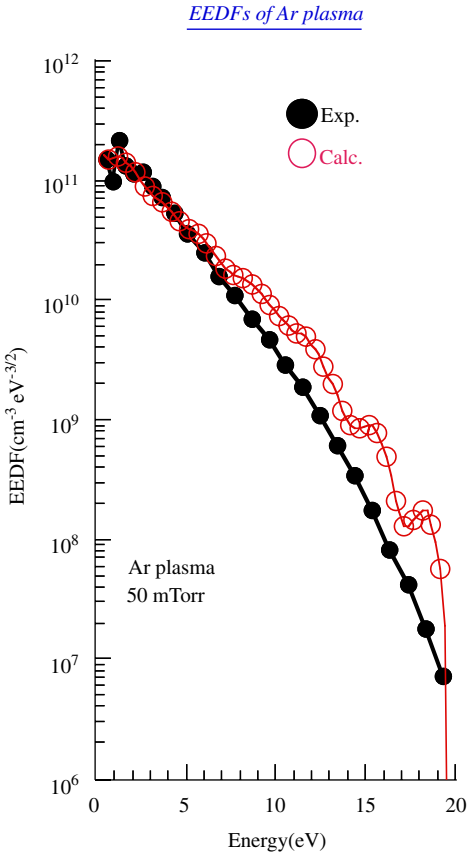

Fig. 9. Measured (closed circles) and calculated (open circles) EEDFs of an Ar plasma at 50 mTorr.

wound around a quartz tube of 40 mm diameter. The procedure of simulation is as follows. The flow, electromagnetic field, and plasma were assumed to be axisymmetric. The calculation was performed by the DSMC method and by electron Monte Carlo simulation. Collisions of e-H, e-H_2, e-CH_4, e-CH_3, e-CH_2, and e-CH were considered in a CH_4/H_2 plasma. The surface reactions of radicals play a critical role in determining the concentrations and distributions of ions and radicals in a reactive plasma such as CH_4/H_2 plasma. The attachment of CH_3, CH_2, and CH radicals on the surface was taken into consideration in the calculation. The sticking coefficients of CH_4, CH_3, and CH_2 radicals used were 1.0×10^{-4}, 1.0×10^{-3}, and 3.0×10^{-2}, as given in previous reports [84–86].

Fig. 9 shows the measured (closed circles) and calculated (open circles) EEDFs of an Ar plasma at 50 mTorr. They nearly form a straight line, which means that the electron energy has a Maxwellian distribution. On the other hand, the EEDFs of a CH_4/H_2 plasma at 50 mTorr are different from those of the Ar plasma at the same pressure. There is a shoulder at approximately 6 eV in both measured (closed circles) and calculated (open circles) EEDFs, as shown in Fig. 10. Turner and Hopkins [87] reported the unusual structure of the EEDF. They found a dip at approximately 4 eV in the EEDF of a N_2 plasma, which is interpreted as the electronic absorption of N_2 molecules corresponding to the resonant peak of the vibrational excitation cross-section. Complex dip/shoulder structures also were found in the EEDFs of N_2 and O_2 molecular plasmas [88]. In the CH_4 vibrational excitation cross-sections, $\sigma_v(1,3)$ and$\sigma_v(2,4)$ have a peak at approximately 6 eV [89]. Therefore, the shoulder at approximately 6 eV can be attributed to the electric absorption of CH_4 molecules analogous to the vibrational absorption of the 4 eV electrons of N_2 molecules. The calculated EEDF of the CH_4/H_2 plasma agrees well with the measured one. Accordingly, the unusual structure at approximately 6 eV in the measured and calculated EEDFs of the CH_4/H_2 plasma can be attributed to inelastic processes involving electrons and the vibrational excitation of CH_4 molecules.

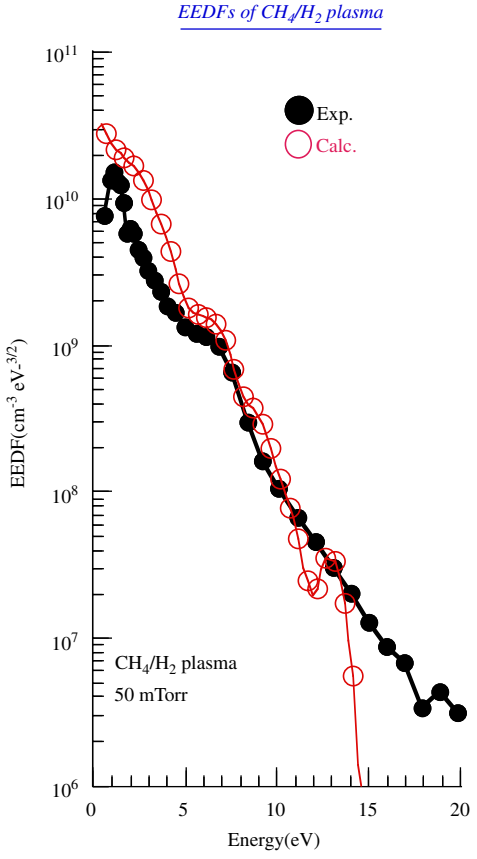

Fig. 10. Measured (closed circles) and calculated (open circles) EEDFs of a CH_4/H_2 plasma at 50 mTorr.

Acknowledgments

The author would like to thank Drs. S. Komatsu, H. Kanda, K. Kimoto, T. Aizawa, R. Souda, and S. Matsumoto of NIMS for their cooperation in experiments and fruitful discussion on the results.

References

[1] J. Robertson, Prog. Solid State Chem. 21 (1991) 199.
[2] M.P. Siegal, W.I. Milne, J.E. Jaskie (Eds.), Covalently bonded disordered thin-film materials, in: Material Research Society Symposium Proceedings, vol. 498, Pittsburgh, PA, 1998.
[3] D.M. Gruen, Annu. Rev. Mater. Sci. 29 (1999) 211.
[4] J. Philip, P. Hess, T. Feygelson, J.E. Butler, S. Chattopadhyay, K.H. Chen, L.C. Chen, J. Appl. Phys. 93 (2003) 2164.
[5] J.A. Carlisle, J. Birrell, J.E. Gerbi, O. Auciello, J.M. Gibson, D.M. Gruen, in: Proceedings of the Eigth International Conference, New Diamond Science and Technology, Melbourne, 2002, 129pp.
[6] G.M. Swain, A.B. Anderson, J.C. Angus, MRS Bull. (1998) 56.
[7] M.A. Lieberman, A.J. Lichtenberg, Principles of Plasma Discharges and Materials Processing, Wiley, New York, 1994.
[8] J. Hopwood, Plasma Sources Sci. Technol. 1 (1992) 109.
[9] J. Amorim, H.S. Maciel, J.P. Sudano, J. Vac. Sci. Technol. B 9 (1991) 362.
[10] M. Kamo, Y. Sato, S. Matsumoto, N. Setaka, J. Cryst. Growth 62 (1983) 642.
[11] R. Erz, W. Dotter, D. Jung, H. Ehrhardt, Diamond Relat. Mater. 2 (1993) 449.
[12] J. Lee, B. Hong, R. Messier, R.W. Collins, Appl. Phys. Lett. 69 (1996) 1716.
[13] T. Sharda, M.M. Rahaman, Y. Nukaya, T. Soga, T. Jimbo, M. Umeno, Diamond Relat. Mater. 10 (2001) 561.
[14] D.M. Gruen, S. Lui, A.R. Krauss, J. Luo, X. Pan, Appl. Phys. Lett. 64 (1994) 1502.
[15] D. Zhou, T.G. McCauley, L.C. Qin, A.R. Krauss, D.M. Gruen, J. Appl. Phys. 83 (1998) 540.
[16] D. Zhou, D.M. Gruen, L.C. Qin, T.G. McCauley, A.R. Krauss, J. Appl. Phys. 84 (1998) 1981.
[17] A.N. Goyette, J.E. Lawler, L.W. Anderson, D.M. Gruen, T.G. McCauley, D. Zhou, A.R. Krauss, J. Phys. D: Appl. Phys. 31 (1998) 1975.
[18] P.C. Redfern, D.A. Horner, L.A. Curtiss, D.M. Gruen, J. Phys. Chem. 100 (1996) 11654.
[19] V.I. Konov, A.A. Smolin, V.G. Ralchenko, S.M. Pimenov, E.D. Obraztsova, Diamond Relat. Mater. 4 (1995) 1073.

[20] A.V. Khomich, V.I. Polyakov, P.I. Perov, V.P. Varnin, I.G. Terenmetskaya, Mater. Res. Soc. Symp. Proc. 423 (1996) 723.
[21] S.N. Kundu, M. Basu, A.B. Maity, S. Chaudhuri, A.K. Pal, Mater. Lett. 31 (1997) 303.
[22] D.V. Fedoseev, V.L. Bukhovets, I.G. Varshavskaya, Y.N. Tolmachev, Russ. J. Phys. Chem. 70 (1996) 1594.
[23] G.A.J. Amaratunga, A. Putnis, K. Clay, W. Milne, Appl. Phys. Lett. 55 (1989) 634.
[24] G.A.J. Amaratunga, S.R.P. Silva, D.A. McKenzie, J. Appl. Phys. 70 (1991) 5374.
[25] P. Badziag, W.S. Verwoerd, W.P. Ellis, N.R. Greiner, Nature 343 (1990) 244.
[26] A.S. Barnard, S.P. Russo, I.K. Snook, Diamond Relat. Mater. 12 (2003) 1867.
[27] J. Wei, H. Kawarada, J. Suzuki, A. Hiraki, J. Cryst. Growth 99 (1990) 1201.
[28] C.R. Eddy, D.L. Youchison, B.D. Sartwell, K.S. Grabowski, J. Mater. Res. 7 (1992) 3255.
[29] M. Zarrabian, N. Fourches-Coulon, G. Turban, C. Marhic, M. Lancin, Appl. Phys. Lett. 70 (1997) 2535.
[30] S.P. Bozeman, D.A. Tucker, B.R. Stoner, J.T. Glass, W.M. Hooke, Appl. Phys. Lett. 66 (1995) 3579.
[31] K. Okada, S. Komatsu, T. Ishigaki, S. Matsumoto, Chemical vapor deposition of refractory metals and ceramics III, in: W.Y. Lee, B.M. Gallois, M.A. Pickering (Eds.), Material Research Society Symposium Proceedings, vol. 363, Pittsburgh, PA, 1995, 157pp.
[32] K. Okada, S. Komatsu, T. Ishigaki, S. Matsumoto, in: Procedings of the 12th International Symposium on Plasma Chemistry, Minnesota, 1995, 2261pp.
[33] K. Okada, S. Komatsu, S. Matsumoto, J. Mater. Res. 14 (1999) 578.
[34] K. Teii, T. Yoshida, J. Appl. Phys. 85 (1999) 1864.
[35] Y. Hirose, Y. Terasawa, Jpn. J. Appl. Phys. 25 (1986) L519.
[36] T. Kawato, K. Kondo, Jpn. J. Appl. Phys. 26 (1987) 1429.
[37] J.A. Mucha, D.L. Flamm, D.E. Ibbotson, J. Appl. Phys. 65 (1989) 3448.
[38] M. Frenklach, H. Wang, Phys. Rev. B 43 (1991) 1520.
[39] K. Teii, H. Ito, M. Hori, T. Takeo, T. Goto, J. Appl. Phys. 87 (2000) 4572.
[40] Y. Kouzuma, K. Teii, K. Uchino, K. Muraoka, Phys. Rev. B 68 (2003) 064104.
[41] S.A. Solin, A.K. Ramdas, Phys. Rev. B 1 (1970) 1687.
[42] R.J. Nemanich, J.T. Glass, G. Lucovsky, R.E. Shroder, J. Vac. Sci. Technol. A 6 (1988) 1783.
[43] J. Wagner, M. Ramsteiner, Ch. Wild, P. Koidl, Phys. Rev. B 40 (1989) 1817.
[44] R.E. Shroder, R.J. Nemanich, Phys. Rev. B 41 (1990) 3738.
[45] F. Tuinstra, J.L. Koenig, J. Chem. Phys. 53 (1970) 1126.
[46] A.C. Ferrari, J. Robertson, Phys. Rev. B 61 (2000) 14095.
[47] M. Nakamizo, R. Kammereck, P.L. Walker Jr., Carbon 12 (1974) 259.
[48] M. Yoshikawa, G. Katagiri, H. Ishida, A. Ishitani, T. Akamatsu, Appl. Phys. Lett. 52 (1988) 1639;
M. Yoshikawa, G. Katagiri, H. Ishida, A. Ishitani, T. Akamatsu, J. Appl. Phys. 64 (1988) 6464.
[49] M. Yoshikawa, N. Nagai, M. Matsuki, H. Fukuda, G. Katagiri, H. Ishida, A. Ishitani, Phys. Rev. B 46 (1992) 7169.
[50] V.I. Merkulov, J.S. Lannin, C.H. Munro, S.A. Asher, V.S. Veerasamy, W.I. Milne, Phys. Rev. Lett. 78 (1997) 4869.
[51] K.W.R. Gilkes, H.S. Sands, D.N. Batchelder, J. Robertson, W.I. Milne, Appl. Phys. Lett. 70 (1997) 1980.
[52] K.W.R. Gilkes, S. Prawer, J. Robertson, H.S. Sands, in: Material Research Society Symposium Proceedings, vol. 498, 1998, 49pp.
[53] D.R. Tallant, T.A. Friedmann, N.A. Missert, M.P. Siegal, J.P. Sullivan, in: Material Research Society Symposium Proceedings, vol. 498, 1998, 37pp.
[54] K. Okada, H. Kanda, S. Komatsu, S. Matsumoto, in: Material Research Society Symposium Proceedings, vol. 593, 2000, 459pp.
[55] Z. Sun, J.R. Shi, B.K. Tay, S.P. Lau, Diamond Relat. Mater. 9 (2000) 1979.
[56] S. Prawer, K.W. Nugent, D.N. Jamieson, J.O. Orwa, L.A. Bursill, J.L. Peng, Chem. Phys. Lett. 332 (2000) 93.
[57] K. Okada, H. Kanda, S. Komatsu, S. Matsumoto, J. Appl. Phys. 88 (2000) 1674.
[58] S. Prawer, K.W. Nugent, in: S.R.P. Silva, J. Robertson, G.A.J. Amaratunga (Eds.), Amorphous Carbon: State of The Art, World Scientific, Singapore, 1998, p. 199.
[59] A.C. Ferrari, J. Robertson, Phys. Rev. B 63 (2001) 121405.
[60] H. Ibach, D.L. Mills, Electron Energy Loss Spectroscopy and Surface Vibrations, Academic Press, London, 1982.
[61] B.J. Waclawski, D.T. Pierce, N. Swanson, R.J. Celotta, J. Vac. Sci. Technol. 21 (1982) 368.
[62] C. Oshima, R. Souda, M. Aono, Y. Ishizawa, Rev. Sci. Instrum. 56 (1985) 227.
[63] C. Oshima, T. Aizawa, R. Souda, Y. Ishizawa, Solid State Commun. 65 (1988) 1601.
[64] T. Aizawa, R. Souda, S. Otani, Y. Ishizawa, C. Oshima, Phys. Rev. Lett. 64 (1989) 768.
[65] T. Aizawa, T. Ando, K. Yamamoto, M. Kamo, Y. Sato, Diamond Relat. Mater. 4 (1995) 600.
[66] K. Okada, T. Aizawa, R. Souda, S. Komatsu, S. Matsumoto, Diamond Relat. Mater. 10 (2001) 1991.
[67] C.Z. Wang, K.M. Ho, Phys. Rev. Lett. 71 (1993) 1184.
[68] D.A. Drabold, P.A. Fedders, P. Stumm, Phys. Rev. B 49 (1994) 16415.
[69] R. Brydson, Electron Energy Loss Spectroscopy, Springer, New York, 2001.
[70] R.F. Egerton, M.J. Whelan, J. Electron. Spectrosc. Relat. Phenom. 3 (1974) 232.
[71] D.A. Muller, Y. Tzou, R. Raj, J. Silcox, Nature 366 (1993) 725.
[72] J. Bruley, D.B. Williams, J.J. Cuomo, D.P. Pappas, J. Microsc. 180 (1995) 22.
[73] L.A. Bursill, J.L. Peng, S. Prawer, Philos. Mag. A 76 (1997) 769.
[74] R.P. Fehlhaber, L.A. Bursill, Philos. Mag. B 79 (1999) 477;
R.P. Fehlhaber, L.A. Bursill, Phys. Rev. B 60 (1999) 14147;
R.P. Fehlhaber, L.A. Bursill, Phys. Rev. B 62 (2000) 17094.
[75] J.L. Peng, R.P. Fehlhaber, L.A. Bursill, D.G. McCulloch, J. Appl. Phys. 89 (2001) 6204.
[76] S. Prawer, J.L. Peng, J.O. Orwa, J.C. McCallum, D.N. Jamieson, L.A. Bursill, Phys. Rev. B 62 (2000) 16360.
[77] K. Okada, K. Kimoto, S. Komatsu, S. Matsumoto, J. Appl. Phys. 93 (2003) 3120.
[78] R. Erz, W. Dotter, D. Jung, H. Ehrhardt, Diamond Relat. Mater. 2 (1993) 449.
[79] P.J. Fallon, L.M. Brown, Diamond Relat. Mater. 2 (1993) 1004.
[80] P. Keblinski, D. Wolf, S.R. Phillpot, H. Gleiter, J. Mater. Res. 13 (1998) 2077.
[81] V. Godyak, in: Proceedings of ICRP-6/SPP-23, Matsushima/Sendai, 2006, p. 1.
[82] K. Okada, S. Komatsu, S. Matsumoto, J. Vac. Sci. Technol. 17 (1999) 721.
[83] K. Okada, S. Komatsu, S. Matsumoto, J. Vac. Sci. Technol. 21 (2003) 1988.
[84] W.L. Hsu, J. Appl. Phys. 72 (1992) 3102.
[85] H. Toyoda, H. Kojima, H. Sugai, Appl. Phys. Lett. 54 (1989) 1507.
[86] H. Kojima, H. Toyoda, H. Sugai, Appl. Phys. Lett. 55 (1989) 1292.
[87] M.M. Turner, M.B. Hopkins, Phys. Rev. Lett. 69 (1992) 3511.
[88] E.I. Toader, Plasma Sources Sci. Technol. 13 (2004) 646.
[89] W.L. Morgan, Plasma Chem. Plasma Process. 12 (1992) 477.